Electrical Power and Energy Systems 162 (2024) 110338

Contents lists available at ScienceDirect

International Journal of Electrical Power and Energy Systems

journal homepage: www.elsevier.com/locate/ijepes

Modeling of small-signal stability margin constrained optimal power flow

Zheng Huang [a], Kewen Wang [a], Yi Wang [a,*], Fushuan Wen [b], Venkata Dinavahi [c], Jun Liang [d]

[a] School of Electrical and Information Engineering, Zhengzhou University, Zhengzhou 450001, China
[b] College of Electrical Engineering, Zhejiang University, Hangzhou 310027, China
[c] Department of Electrical and Computer Engineering, University of Alberta, Edmonton, AB T6G 2V4, Canada
[d] School of Engineering, Cardiff University, Cardiff CF24 3AA, UK

ARTICLE INFO

Keywords:
Damping ratio
Eigenvalue
Optimal power flow
Power system computation
Small-signal stability
Stability margin

ABSTRACT

This paper presents a novel small-signal stability margin (SSSM) constrained optimal power flow model for generation dispatch to minimize the generation cost while retaining adequate SSSM. The SSSM constraint is described in terms of the total active load variation between an initial operating point and the critical point, which is located on the dynamic performance boundary of small-signal stability. From the existing SSSM model, where the steady-state equation and the small-signal stability equation are taken into account, a modified SSSM model is proposed to reduce the computational requirement. The sensitivity representation of SSSM with respect to operating parameters is newly derived, which makes it possible for the SSSM and steady-state optimization problems to be jointly solved. A joint solution approach is proposed to solve the small-signal stability margin constrained optimal power flow (SSSMC-OPF) model. Simulation results show that the proposed approach can effectively minimize the generation cost subject to retaining a certain level of SSSM. For an 8-machine 24-bus system and a modified practical 68-machine 2395-bus system, the generation costs of SSSMC-OPF are increased by 5.28% and 2.73%, respectively, but the SSSMs are improved by 45% and 14.41%, respectively, compared to the optimal power flow.

1. Introduction

1.1. Motivation

Optimal power flow (OPF) has become a powerful tool for modern power system operation and planning [1–3]. However, the increased penetration of renewable energy resources [4,5] and energy storages [6,7] in power systems will have a significant impact on both the grid structure and the power flow distribution, which may lead to inadequate damping behaviour or even instability. If stability requirements are not met by the results obtained from the traditional OPF, generation re-dispatch is required. With the development of computer technology and optimization methodologies, stability conditions can also be incorporated into the traditional OPF model [8,9]. Small-signal stability constrained optimal power flow (SSSC-OPF) has gained attention in recent years [10], as the SSSC-OPF can provide the complete rescheduling information while considering the economic objectives and small-signal stability constraints.

1.2. Literature review

Typically, the small-signal stability constraint can be formed by the eigenvalues and/or damping ratios of electromechanical oscillation modes. A small-signal stability constraint, described by the minimum damping ratio, was first introduced in the optimization model by [11], which sought to maximize the power transfer without violating the small-signal stability constraint. In [12], the small-signal stability constraint was formulated based on the real part of critical eigenvalues, which was incorporated into the optimal power flow model and solved by the primal–dual interior point method. The potential of reactive power to improve the dynamic performance of power systems was investigated in [13]. Since eigenvalues considered in the small-signal stability constraint may change during the iteration process, a gradient sampling theory was introduced in [14] to efficiently solve the SSSC-OPF model, and a sequential approach was proposed in [15] to approach the optimal operating point step-by-step. To reduce the computational requirement of solving the SSSC-OPF problem, stability constraints were developed in [16–18] using a bilinear matrix inequality

* Corresponding author.
E-mail addresses: huangzheng1535@163.com (Z. Huang), kwwang@zzu.edu.cn (K. Wang), yiwang@zzu.edu.cn (Y. Wang), fushuan.wen@gmail.com (F. Wen), dinavahi@ualberta.ca (V. Dinavahi), LiangJ1@cardiff.ac.uk (J. Liang).

https://doi.org/10.1016/j.ijepes.2024.110338
Received 11 March 2024; Received in revised form 10 July 2024; Accepted 22 October 2024
Available online 30 October 2024

approach, which avoids the repeated calculation of eigenvalues and their sensitivities. In [19], a data-driven small-signal stability constraint, expressed as an explicit function of generator voltages, was also developed and included in the OPF model.

Currently, most small-signal stability constrained optimization problems have focused on the stability and/or dynamic performance at an operating point [10–20]. However, for practical power systems, it is obviously more reasonable and intuitive to retain a certain small-signal stability margin (SSSM). The SSSM is described by the relationship between an initial operating point and the critical point, in which the critical point is located on the stability boundary or dynamic performance boundary of small-signal stability. Progress has been made in understanding the SSSM and monitoring the critical mode first crosses the imaginary axis or damping ratio line with various approaches. For example, the optimization technique [21] and the rightmost eigenvalue tracing approach [22] have been utilized to identify the critical point and compute the SSSM. To date, the three-stage strategy [23], namely the estimation stage, correction stage, and verification stage, has been the most effective method for computing the SSSM under a given direction of load and generation variation.

Extensive research works have focused on voltage stability margin constrained optimal power flow (VSMC-OPF) problems [24,25], but there is still little research on small-signal stability margin constrained optimal power flow (SSSMC-OPF) problems. In [26], the SSSM constraint was defined using a second-order approximation approach for measuring the distance from an initial operating point to the critical point, which is located on the small-signal stability boundary. The conditions that power systems must satisfy at the critical point are composed of the steady-state equation and the requirement of the largest real part of critical modes. In [27], this SSSM constraint was incorporated into stochastic optimal power flow model to minimize the operating cost. The taxonomy of aforementioned literatures is shown in Table 1.

1.3. Research gaps

Based on the research background and Table 1, it is evident that the following research gaps exist in the field of SSSMC-OPF problems.

Many publications have discussed the small-signal stability constrained operation optimization problems [10–20], SSSM problems [21–23,26], and VSMC-OPF problems [24,25,27], but there is still little research on SSSMC-OPF problems [26,27].

In the formation of the SSSM constraint in [26] and [27], the requirement of the largest real part of critical modes at the critical point was considered, but the damping ratio requirement was not taken into account. Furthermore, the SSSM constraint was defined using a second-order approximation approach.

1.4. Contributions

In order to fill these research gaps, this paper proposes a novel OPF model with exact SSSM constraint. The SSSM constraint is defined based on the total active load variation between an initial operating point and the critical point, which is located on the dynamic performance boundary of small-signal stability. From the existing SSSM model, where the steady-state and the minimum damping ratio requirements are considered, a modified SSSM model is developed to reduce the computational requirement. A joint solution approach is designed to effectively solve the SSSMC-OPF model, where the sensitivity representation of SSSM with respect to operating parameters is newly derived and utilized to guide the optimization direction. The main contributions are summarized as follows, and the graphical abstract as shown in Fig. 1.

(1) A novel OPF model with exact SSSM constraint is proposed for generation dispatch to minimize the operating cost while retaining the system with a given SSSM.
(2) A joint solution approach is developed to effectively solve the SSSMC-OPF model, and the conflicting relationship between generation cost and SSSM is revealed.
(3) Based on a modified SSSM model, the analytical representation of the SSSM sensitivities with respect to operating parameters is newly derived, which can be used for SSSM analysis and control, SSSM constrained optimization problems, among other applications.

1.5. Paper organization

The remainder of this paper is organized as follows. In Section 2, the system dynamic model considering the load and generation variation is presented. The modified SSSM model is presented in Section 3. In Section 4, the proposed SSSMC-OPF model is introduced. In Section 5, a joint solution approach for the proposed model, as well as the SSSM sensitivities, are given in detail. In Section 6, the effectiveness of the proposed approach is tested and validated on an 8-machine system and a modified practical system. Finally, the conclusions are drawn in Section 7.

2. System dynamic model considering the load and generation variation

Generally, the load and generation variation can be expressed as [23,28]:

$$\begin{cases} \boldsymbol{P}_{\mathrm{L}} = \boldsymbol{P}_{\mathrm{L}}^{\mathrm{N}} + \mu \boldsymbol{B}_{\mathrm{L}}^{\mathrm{P}} \\ \boldsymbol{Q}_{\mathrm{L}} = \boldsymbol{Q}_{\mathrm{L}}^{\mathrm{N}} + \mu \boldsymbol{B}_{\mathrm{L}}^{\mathrm{Q}} \\ \boldsymbol{P}_{\mathrm{G}} = \boldsymbol{P}_{\mathrm{G}}^{\mathrm{N}} + \mu \boldsymbol{B}_{\mathrm{G}}^{\mathrm{P}} \end{cases}, \tag{1}$$

where $\boldsymbol{P}$ and $\boldsymbol{Q}$, respectively, denote column vectors of active and reactive power. $\boldsymbol{B}$ indicates the column vector describing the direction of power variation, which can be determined by the short-term forecasting of load demands and the generation rescheduling scheme [23]. μ represents a scalar parameter subject to variation. Superscripts "P" and "Q" represent active and reactive power, respectively. Subscripts "L" and "G"

Table 1
Comparison of the Literature with This Paper.

Ref.	SSSC-OO	VSMC-OPF	SSSM		SSSMC-OPF	
			LRP	MDR	LRP	MDR
[10–20]	Yes	No	No	No	No	No
[21–23]	No	No	Exact	Exact	No	No
[24,25]	No	Yes	No	No	No	No
[26]	No	No	Second-order approximation	No	No	No
[27]	No	Second-order approximation	No	No	Second-order approximation	No
This paper	No	No	No	No	Exact	Exact

SSSC-OO: small-signal stability constrained operation optimization, LRP: Largest real part of critical modes, MDR: minimum damping ratio of critical modes.

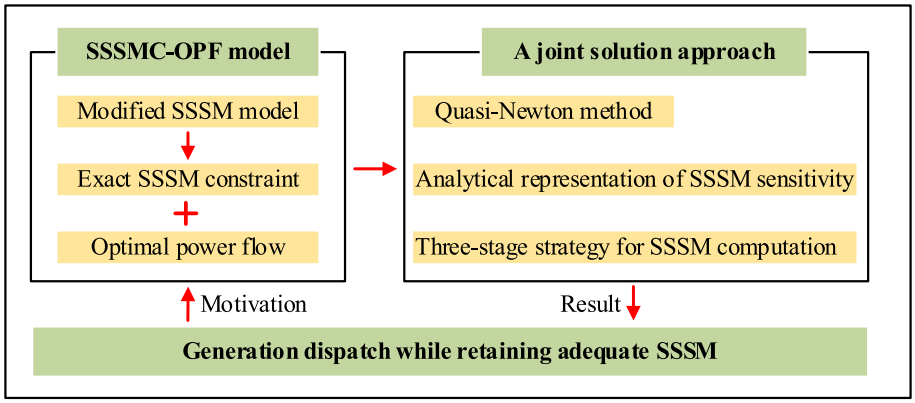

Fig. 1. Graphical abstract.

denote load and generator buses, respectively. Superscript "N" stands for the initial operating point. $\boldsymbol{P}_{\mathrm{L}}$, $\boldsymbol{Q}_{\mathrm{L}}$, and $\boldsymbol{P}_{\mathrm{G}}$ represent power vectors at arbitrary operating point.

The differential–algebraic equations of power systems used for stability analysis, taking into account the variation of power, can be expressed as

$$\dot{\boldsymbol{x}} = \boldsymbol{F}_{\mathrm{d}}(\boldsymbol{x}, \boldsymbol{m}), \tag{2a}$$

$$\boldsymbol{0} = \boldsymbol{G}_{\mathrm{a}}(\boldsymbol{x}, \boldsymbol{m}, \mu), \tag{2b}$$

where $\boldsymbol{x}$ and $\boldsymbol{m}$ denote column vectors of state and non-state variables, respectively. $\boldsymbol{F}_{\mathrm{d}}$ and $\boldsymbol{G}_{\mathrm{a}}$ describe the differential and algebraic relations in power systems, respectively. In (2b), (1) is taken into account.

Let $\dot{\boldsymbol{x}}_1 = \left[\dot{\boldsymbol{x}}^{\mathrm{T}}\ \boldsymbol{0}\right]^{\mathrm{T}}$ and $\boldsymbol{F}_1 = \left[\boldsymbol{F}_{\mathrm{d}}^{\mathrm{T}}\ \boldsymbol{G}_{\mathrm{a}}^{\mathrm{T}}\right]^{\mathrm{T}}$. For convenience, (2) can be simplified as

$$\dot{\boldsymbol{x}}_1 = \boldsymbol{F}_1(\boldsymbol{x}, \boldsymbol{m}, \mu). \tag{3}$$

The state space equation (4) at the given parameter μ can be obtained by linearizing (3) and eliminating the non-state vector $\boldsymbol{m}$.

$$\Delta\dot{\boldsymbol{x}} = \boldsymbol{A}\Delta\boldsymbol{x}, \tag{4}$$

where $\boldsymbol{A}$ represents the state matrix, Δ indicates tiny changes.

The eigenvalues of $\boldsymbol{A}$ are typically used for small-signal stability analysis. For an oscillatory mode corresponding to complex eigenvalues $\lambda = \sigma \pm \mathrm{j}\omega$, the damping ratio ζ can be obtained by

$$\zeta = -\frac{\sigma}{\sqrt{\sigma^2 + \omega^2}}, \tag{5}$$

where σ and ω denote the real and imaginary parts of the eigenvalue λ, respectively.

3. Modified SSSM model

In this section, first, the SSSM model is introduced, which takes into account the steady-state equation and the small-signal stability equation. More importantly, a modified SSSM model is then proposed.

3.1. SSSM index

Assuming that the minimum damping ratio of an initial operating point is greater than ζ_{T} at $\mu = 0$. As μ increases, the initial operating point will change. When a pair of eigenvalues reach the damping ratio line ζ_{T} at $\mu = \mu_{\mathrm{C}}$ first, the operating point is defined as the critical point located at the dynamic performance boundary. In this case, if $\zeta_{\mathrm{T}} = 0$, the critical point is located at the small-signal stability boundary. Thus, the SSSM can be defined as the percentage change in the total active load for a given direction of power variation that would cause the damping ratio to reach its minimum limit. Mathematically, the SSSM index γ can be described as

$$\gamma = \frac{P_{\mathrm{L},\Sigma}^{\mathrm{C}} - P_{\mathrm{L},\Sigma}^{\mathrm{N}}}{P_{\mathrm{L},\Sigma}^{\mathrm{N}}} \times 100\%, \tag{6}$$

where $P_{\mathrm{L},\Sigma}^{\mathrm{N}}$ and $P_{\mathrm{L},\Sigma}^{\mathrm{C}}$ denote the total active load at the initial operating point and the critical point, respectively. The relationship between $P_{\mathrm{L},\Sigma}^{\mathrm{N}}$ and $P_{\mathrm{L},\Sigma}^{\mathrm{C}}$ can be derived from the first equation in (1) as

$$P_{\mathrm{L},\Sigma}^{\mathrm{C}} = P_{\mathrm{L},\Sigma}^{\mathrm{N}} + \mu B_{\mathrm{L},\Sigma}^{\mathrm{P}}, \tag{7}$$

where $B_{\mathrm{L},\Sigma}^{\mathrm{P}}$ represents the sum of all elements in vector $\boldsymbol{B}_{\mathrm{L}}^{\mathrm{P}}$.

By substituting (7) into (6), (6) can be reformulated as

$$\gamma = \mu \frac{B_{\mathrm{L},\Sigma}^{\mathrm{P}}}{P_{\mathrm{L},\Sigma}^{\mathrm{N}}} \times 100\%, \tag{8}$$

From (8), with a specific direction of the load and generation variation, the SSSM index is determined by μ. The SSSM index in (6) or (8) visually describes the power variation that a power system can withstand at an initial operating point. If the SSSM index is greater than zero, the system is in an adequate damping condition along a specific direction of power variation from the initial operating point to the critical point.

3.2. SSSM model

Let $\widetilde{\lambda}_{\mathrm{m}} = \widetilde{\sigma}_{\mathrm{m}} \pm \mathrm{j}\widetilde{\omega}_{\mathrm{m}}$ denotes the eigenvalue corresponding to the minimum damping ratio at the critical point with the right eigenvector $\widetilde{\boldsymbol{U}} = \widetilde{\boldsymbol{U}}_{\mathrm{Re}} \pm \mathrm{j}\widetilde{\boldsymbol{U}}_{\mathrm{Im}}$. The steady-state equation and the small-signal stability equation that must be satisfied simultaneously at the critical point are as follows [23]

$$\boldsymbol{F}_1(\widetilde{\boldsymbol{x}}, \widetilde{\boldsymbol{m}}, \widetilde{\mu}) = \boldsymbol{0}, \tag{9a}$$

$$\boldsymbol{A}\widetilde{\boldsymbol{U}}_{\mathrm{Re}} - \widetilde{\sigma}_{\mathrm{m}}\widetilde{\boldsymbol{U}}_{\mathrm{Re}} + \widetilde{\omega}_{\mathrm{m}}\widetilde{\boldsymbol{U}}_{\mathrm{Im}} = \boldsymbol{0}, \tag{9b}$$

$$\boldsymbol{A}\widetilde{\boldsymbol{U}}_{\mathrm{Im}} - \widetilde{\sigma}_{\mathrm{m}}\widetilde{\boldsymbol{U}}_{\mathrm{Im}} - \widetilde{\omega}_{\mathrm{m}}\widetilde{\boldsymbol{U}}_{\mathrm{Re}} = \boldsymbol{0}, \tag{9c}$$

$$\boldsymbol{U}_{\mathrm{Re}}^{\mathrm{T}}\widetilde{\boldsymbol{U}}_{\mathrm{Re}} + \boldsymbol{U}_{\mathrm{Im}}^{\mathrm{T}}\widetilde{\boldsymbol{U}}_{\mathrm{Im}} - 1 = 0, \tag{9d}$$

$$\boldsymbol{U}_{\mathrm{Re}}^{\mathrm{T}}\widetilde{\boldsymbol{U}}_{\mathrm{Im}} - \boldsymbol{U}_{\mathrm{Im}}^{\mathrm{T}}\widetilde{\boldsymbol{U}}_{\mathrm{Re}} = 0, \tag{9e}$$

$$\widetilde{\sigma}_{\mathrm{m}} / \sqrt{\widetilde{\sigma}_{\mathrm{m}}^2 + \widetilde{\omega}_{\mathrm{m}}^2} + \zeta_{\mathrm{T}} = 0, \tag{9f}$$

where symbols $\boldsymbol{x}$, $\boldsymbol{m}$, and μ are the same as that in (2), symbol "~" indicates the critical point, superscript "T" denotes the transpose of the matrix, (9a) represents the steady-state operating condition, (9b) and

(9c) indicate the characteristic equation on the real domain, (9d) and (9e) denote the normalized equation on the real domain, and (9f) represents the minimum damping ratio requirement. All unknown variables in (9) can be collected in a vector $\boldsymbol{y}_1$ defined as

$$\boldsymbol{y}_1 = [\widetilde{\boldsymbol{x}}^{\mathrm{T}}, \widetilde{\boldsymbol{m}}^{\mathrm{T}}, \widetilde{\boldsymbol{U}}_{\mathrm{Re}}^{\mathrm{T}}, \widetilde{\boldsymbol{U}}_{\mathrm{Im}}^{\mathrm{T}}, \widetilde{\sigma}_{\mathrm{m}}, \widetilde{\omega}_{\mathrm{m}}, \widetilde{\mu}]^{\mathrm{T}}. \tag{10}$$

Let N_{S} and N_{M} stand for the number of elements in state vector $\widetilde{\boldsymbol{x}}$ and non-state vector $\widetilde{\boldsymbol{m}}$, respectively. The total number of elements in $\boldsymbol{y}_1$ is $3N_{\mathrm{S}} + N_{\mathrm{M}} + 3$, which is equal to the dimension of (9). For large-scale systems with a large number of state and non-state variables, the solution of (9) is computationally intensive. To reduce the computational requirement without compromising the results, a modified SSSM model is proposed in the next section, in which the number of equations and variables in (9a) are reduced.

3.3. Modified SSSM model

Equation (9a) is utilized to determine the operation state of a power system, i.e., determine the values of all state and non-state variables. However, the operation state of the power system can also be completely determined by partial state and non-state variables. Since the values of controller variables do not change in steady-state, controller equations are ineffective in steady-state operation of the system. Therefore, a large number of controller equations contained in (9a) can be excluded.

For a system of N_{G}-machine, only partial state and non-state variables are required, which can be collected in a vector $\boldsymbol{y}_2$ in (11) with subvector $\boldsymbol{M}_{1(i)}$ corresponding to ith machine, $\boldsymbol{V}$ collecting the real and imaginary parts of all the nodal voltages except the slack bus, and $\boldsymbol{I}_{\mathrm{G}}$ collecting the real and imaginary parts of all the generator nodal currents.

$$\boldsymbol{y}_2 = [\boldsymbol{M}_{1(1)}, \cdots, \boldsymbol{M}_{1(i)}, \cdots, \boldsymbol{M}_{1(N_{\mathrm{G}})}, \boldsymbol{V}^{\mathrm{T}}, \boldsymbol{I}_{\mathrm{G}}^{\mathrm{T}}]^{\mathrm{T}}, \tag{11a}$$

$$\boldsymbol{M}_{1(i)} = [I_{di}, I_{qi}, V_{di}, V_{qi}, \delta_i], \tag{11b}$$

where subscripts "d" and "q" refer to the machine dq frame, δ indicates the power angle measured with respect to the reference machine.

To completely determine the value of all elements in vector $\boldsymbol{y}_2$, the power flow equation can be combined with the following equation

$$\boldsymbol{I}_{\mathrm{G}} = [\boldsymbol{Y}_{\mathrm{GG}} \boldsymbol{Y}_{\mathrm{GL}}]\boldsymbol{V}, \tag{12a}$$

$$V_{qi}\cos\delta_i + V_{di}\sin\delta_i - V_{xi} = 0, \tag{12b}$$

$$V_{qi}\sin\delta_i - V_{di}\cos\delta_i - V_{yi} = 0, \tag{12c}$$

$$I_{xi}\cos\delta_i + I_{yi}\sin\delta_i - I_{qi} = 0, \tag{12d}$$

$$I_{xi}\sin\delta_i - I_{yi}\cos\delta_i - I_{di} = 0, \tag{12e}$$

$$\arctan(E_{Qyi}/E_{Qxi}) - \delta_i = 0, \tag{12f}$$

where subscripts "x" and "y" refer to the network frame, $\boldsymbol{Y}_{\mathrm{GG}}$ and $\boldsymbol{Y}_{\mathrm{GL}}$ represent the submatrices of the nodal admittance matrix $\boldsymbol{Y}$ corresponding to the generator, E_Q denote the virtual electromotive force, (12a) indicates the network equation, (12b)–(12e) denote the coordinate transformation, and (12f) represents the power angle equation. E_{Qxi} and E_{Qyi} can be expressed by

$$E_{Qxi} = V_{xi} + R_{ai}I_{xi} - X_{qi}I_{yi}, \tag{12g}$$

$$E_{Qyi} = V_{yi} + R_{ai}I_{yi} + X_{qi}I_{xi}, \tag{12h}$$

where R_a and X_q represent stator resistance and synchronous reactance, respectively. For convenience, the power flow equation and (12) at the critical point can be simply expressed as

$$\boldsymbol{F}_2(\widetilde{\boldsymbol{y}}_2, \widetilde{\mu}) = \boldsymbol{0}. \tag{13}$$

Unlike (9a), ineffective controller equations under steady-state are not included in (13). Therefore, a modified SSSM model is formed by using (13) instead of (9a). For a system of N_{G}-machine and N_{B}-bus, the vector $\boldsymbol{y}_3$ collecting all unknown variables of the modified SSSM model has the form of

$$\boldsymbol{y}_3 = [\widetilde{\boldsymbol{y}}_2^{\mathrm{T}}, \widetilde{\boldsymbol{U}}_{\mathrm{Re}}^{\mathrm{T}}, \widetilde{\boldsymbol{U}}_{\mathrm{Im}}^{\mathrm{T}}, \widetilde{\sigma}_{\mathrm{m}}, \widetilde{\omega}_{\mathrm{m}}, \widetilde{\mu}]^{\mathrm{T}}. \tag{14}$$

The total number of elements in $\boldsymbol{y}_2$ or $\widetilde{\boldsymbol{y}}_2$ is $2N_{\mathrm{B}} + 7N_{\mathrm{G}}$-2, while the total number of elements in $\boldsymbol{y}_3$ is $2N_{\mathrm{B}} + 7N_{\mathrm{G}} + 2N_{\mathrm{S}} + 1$. The number of equations in the modified SSSM model is the same as the number of unknown variables. Results of the modified SSSM model are consistent with the SSSM model, but the number of equations in the modified SSSM model is reduced by $N_{\mathrm{S}} + N_{\mathrm{M}}$-$2N_{\mathrm{B}}$-$7N_{\mathrm{G}} + 2$. For a modified practical system in Section 6.2, the number of equations in the modified SSSM model is reduced by 2417 compared to the SSSM model with the equations being 10124.

4. Optimal power flow model with an exact SSSM constraint

In this section, first, a novel SSSMC-OPF model is proposed for generation dispatch in order to minimize the generation cost subject to an exact SSSM constraint under a given direction of power variation. The differences between the presented model and existing models are then analyzed.

It should be noted that from the perspective of the stability analysis, the SSSM is defined based on the relationship between an initial operating point and the critical point. However, both steady-state optimization and SSSM problems are included in the SSSMC-OPF problem. For the convenience in later presentation, in this paper, the initial operating point includes operating points before and after optimization.

4.1. SSSMC-OPF model

In order to incorporate an exact SSSM limit into the standard OPF model, several modeling techniques can be used [24,29,30]. For example, the SSSM condition may be modeled as an inequality constraint, or as one of the objective functions, etc. In this paper, the SSSM condition is considered as an inequality constraint to be included in the standard OPF model. The objective function and all constraints used in the SSSMC-OPF problem are described in detail below.

1) Objective Function: Minimizing the generation cost is considered as the objective function in this paper, which may be expressed as (15). Note that other objective functions can also be used, such as minimizing the generation adjustment cost or minimizing the active power adjustment.

$$\min f = \sum_{i=1}^{N_{\mathrm{G}}} \left(a_i (P_{\mathrm{G}i}^{\mathrm{N}})^2 + b_i P_{\mathrm{G}i}^{\mathrm{N}} + c_i \right), \tag{15}$$

where a_i, b_i, and c_i denote cost coefficients of the ith generator.

2) Power Flow Equations at an Initial Operating Point:

$$P_{\mathrm{G}i}^{\mathrm{N}} - P_{\mathrm{L}i}^{\mathrm{N}} = V_i^{\mathrm{N}} \sum_{j=1}^{N_{\mathrm{B}}} V_j^{\mathrm{N}} (G_{ij}\cos\theta_{ij}^{\mathrm{N}} + B_{ij}\sin\theta_{ij}^{\mathrm{N}}), \tag{16}$$

$$Q_{\mathrm{G}i}^{\mathrm{N}} - Q_{\mathrm{L}i}^{\mathrm{N}} = V_i^{\mathrm{N}} \sum_{j=1}^{N_{\mathrm{B}}} V_j^{\mathrm{N}} (G_{ij}\sin\theta_{ij}^{\mathrm{N}} - B_{ij}\cos\theta_{ij}^{\mathrm{N}}), \tag{17}$$

where G_{ij} and B_{ij} represent the real and imaginary parts of the ith row, jth column element in the nodal admittance matrix, respectively, $\theta_{ij}^{\mathrm{N}} = \theta_i^{\mathrm{N}} - \theta_j^{\mathrm{N}}$, V_i^{N} and θ_i^{N} indicate the voltage magnitude and angle of bus i at an initial point, respectively.

3) Technical Limits at an Initial Operating Point:

$$P_{Gi}^{\min} \le P_{Gi}^{N} \le P_{Gi}^{\max}, \tag{18}$$

$$Q_{Gi}^{\min} \le Q_{Gi}^{N} \le Q_{Gi}^{\max}, \tag{19}$$

$$V_{i}^{\min} \le V_{i}^{N} \le V_{i}^{\max}, \tag{20}$$

$$(I_{ij}^{N})^2 \le (I_{ij}^{\max})^2, \tag{21}$$

where superscripts "min" and "max" denote the lower and upper limits, respectively, and I_{ij}^{N} represents the current between buses i and j.

4) SSSM Constraint: In general, power systems should not approach their stability limits, but a certain margin should be retained [31]. The SSSM limit of a power system can be expressed by an inequality constraint as

$$\gamma \ge \gamma_{\min}, \tag{22}$$

where γ can be computed from the modified SSSM model in Section 3, $\gamma_{\min}$ can be determined according to the system operational requirement or related standards.

4.2. Relation to the existing models

In [10–20], only the stability and/or dynamic performance are considered in the small-signal stability constrained optimization models. The generation dispatch information obtained by the proposed SSSMC-OPF model not only ensures the dynamic performance, but also provides the power variation that a power system can withstand.

Regarding the construction of SSSM constraints, the SSSM constraint in [27] requires that the critical point to be located at the stability boundary, while (22) requires that the critical point to be located at the dynamic performance boundary. In addition, the SSSM constraint in [27] was described by a second-order approximation approach, while (22) is an accurate representation. Compared to the existing models, the proposed SSSMC-OPF model is more intuitive and reasonable.

5. A joint solution approach for SSSMC-OPF

The SSSMC-OPF model (15)–(22) is a nonlinear programming problem that can be solved by many mature algorithms (e.g., deterministic algorithms, non-deterministic algorithms) [32,33]. Generally speaking, deterministic algorithms can generate reasonable optimal solutions with excellent computational speed. Conventionally, deterministic algorithms can be classified into two categories: alternating solution techniques and joint solution techniques [32]. Compared with alternating solution techniques, joint solution techniques have advantages in convergence and computational speed.

However, the complexity of solving the SSSMC-OPF model using joint solution techniques is significantly increased by the following two reasons.

(1) The computation of SSSM index in (22) is quite complex because the steady-state equation and the small-signal stability equation are included in the modified SSSM model.
(2) The sensitivities of the SSSM with respect to operating parameters are necessary for the joint solution of the SSSM and OPF problems. Existing SSSM sensitivity calculations are mainly related to the small-signal stability boundary [20,26], and must be extended to the dynamic performance boundary.

In this section, first, a joint solution approach for the SSSMC-OPF problem is proposed. The analytical representation of the SSSM sensitivities with respect to operating parameters is then derived.

5.1. Problem reformulation

The SSSMC-OPF problem can be compactly rewritten as

$$\min f(\boldsymbol{u}) \tag{23}$$

$$\text{s.t. } \boldsymbol{h}(\boldsymbol{u}) = \boldsymbol{0} \tag{24}$$

$$\boldsymbol{g}(\boldsymbol{u}) \le \boldsymbol{0}, \tag{25}$$

where $\boldsymbol{u}$ denotes the column vector of control variables composed of the active power output P_{Gi}^{N} and the voltage magnitude V_{Gi}^{N} of all generators except for the slack generator,f represents the objective function, $\boldsymbol{h}$ and $\boldsymbol{g}$ indicate the vectors corresponding to the equality and inequality constraints, respectively.

It should be noted that the SSSM constraint (22) is an implicit function of $\boldsymbol{u}$ and can also be included in (25). This is because the SSSM constraint (22) is defined under a given direction of power variation, and if $\boldsymbol{u}$ is given, the SSSM index γ can be computed from (9b)–(9f), (13), as well as (6) or (8).

5.2. Problem solution

Various optimization techniques could be used for the joint solution of the SSSMC-OPF problem [32]. Since the second-order SSSM sensitivity calculation is very complicated, in this paper, the quasi-Newton technique is used because of its simplicity and ease of implementation [34,35]. An augmented Lagrangian function can be formed as

$$L(\boldsymbol{u},\boldsymbol{z}) = f(\boldsymbol{u}) + \boldsymbol{z}^{\mathrm{T}}\boldsymbol{h}(\boldsymbol{u}) + \sum_{i=1}^{r} [\ell_i \cdot \max\{0, g_i(\boldsymbol{u})\}]^2, \tag{26}$$

where $\boldsymbol{z}$ denotes the vector of Lagrangian multipliers, ℓ_i indicates the penalty factor for the ith inequality constraint, and r represents the total number of inequality constraints in (25).

With $\boldsymbol{K} = [\boldsymbol{u}^{\mathrm{T}}\ \boldsymbol{z}^{\mathrm{T}}]^{\mathrm{T}}$, the Karush-Kuhn-Tucker (KKT) condition of the augmented Lagrangian function of (26) can be derived as

$$\begin{cases} \nabla_{\boldsymbol{u}} L(\boldsymbol{K}) = \boldsymbol{0} \\ \nabla_{\boldsymbol{z}} L(\boldsymbol{K}) = \boldsymbol{0} \end{cases}, \tag{27}$$

where $\nabla_{\boldsymbol{u}} L$ and $\nabla_{\boldsymbol{z}} L$ are gradient vectors of the Lagrangian with respect to control vector and Lagrangian multipliers vector, respectively.

The correction equations of the KKT condition can be written under the quasi-Newton technique as

$$\boldsymbol{K}^{(l+1)} = \boldsymbol{K}^{(l)} - \eta^{(l)} \boldsymbol{H}^{(l)} \nabla L(\boldsymbol{K}^{(l)}), \tag{28}$$

where the superscript "l" indicates the iteration number of the quasi-Newton technique, η denotes the optimal step length obtained using the one-dimensional search [34], and $\boldsymbol{H}^{(l)}$ represents the approximation inverse of Hessian matrix of the Lagrangian of (26) at the operation point $\boldsymbol{K}^{(l)}$. $\boldsymbol{H}^{(l)}$ is improved in this paper by the popular Broyden-Fletcher-Goldfarb-Shanno (BFGS) technique [34].

5.3. Computation of the SSSM index

The SSSM index will be used in the computation of the value of the augmented Lagrangian function (26). However, how to efficiently solve the modified SSSM model is a problem. As discussed in Section 3.3, the number of equations in the modified SSSM model is the same as the number of unknown variables, it can be solved by using the Newton method or its variants. However, since the steady-state equation and the small-signal stability equation are included in the modified SSSM model, it may fail to converge if appropriate initial values are not provided.

To deal with this problem, a three-stage strategy was proposed in [23]. In the first stage, the critical eigenvalue that first crosses the damping ratio line was determined; in the second stage, the exact SSSM

can be obtained by the Newton method; in the third stage, computational results were verified. The three-stage strategy is utilized to solve the modified SSSM model in this paper.

5.4. SSSM sensitivities

The SSSM sensitivities with respect to variables in vector $\boldsymbol{K}$ will be used in the calculation of the gradient vector in (27). Since the SSSM sensitivities with respect to the Lagrangian multipliers vector $\boldsymbol{z}$ in $\boldsymbol{K}$ are 0, the analytical sensitivity representation of the SSSM with respect to the control vector $\boldsymbol{u}$ in $\boldsymbol{K}$ is described in detail below.

For arbitrary parameter in vector $\boldsymbol{u}$, such as κ_i, the derivative of the SSSM index γ can be derived from (6) or (8) as

$$\frac{\partial\gamma}{\partial\kappa_i}=\left(\frac{\partial\widetilde{\mu}}{\partial\kappa_i}\frac{B^{\mathrm{P}}_{\mathrm{L},\Sigma}}{P^{\mathrm{N}}_{\mathrm{L},\Sigma}}+\frac{\widetilde{\mu}}{P^{\mathrm{N}}_{\mathrm{L},\Sigma}}\frac{\partial B^{\mathrm{P}}_{\mathrm{L},\Sigma}}{\partial\kappa_i}-\frac{\widetilde{\mu}B^{\mathrm{P}}_{\mathrm{L},\Sigma}}{\left(P^{\mathrm{N}}_{\mathrm{L},\Sigma}\right)^2}\frac{\partial P^{\mathrm{N}}_{\mathrm{L},\Sigma}}{\partial\kappa_i}\right)\times 100\%. \tag{29}$$

$\partial B^{\mathrm{P}}_{\mathrm{L},\Sigma}/\partial\kappa_i$ is related to the direction of power variation, and $\partial P^{\mathrm{N}}_{\mathrm{L},\Sigma}/\partial\kappa_i$ is related to the load model. Both are easy to obtain, while $\partial\widetilde{\mu}/\partial\kappa_i$ is relatively complicated. Since $\widetilde{\mu}$ is the last element in vector $\boldsymbol{y}_3$ of (14), $\partial\widetilde{\mu}/\partial\kappa_i$ in $\partial\boldsymbol{y}_3/\partial\kappa_i$ can be derived from (9b)–(9f) and (13). For convenience, (9b)–(9f) and (13) can be rewritten compactly as

$$\boldsymbol{G}(\boldsymbol{y}_3)=\boldsymbol{0}. \tag{30}$$

The derivative of $\boldsymbol{y}_3$ will be obtained from the differentiation of (30) using the differential chain rule and expressed as

$$\frac{\partial\boldsymbol{y}_3}{\partial\kappa_i}=-\boldsymbol{J}^{-1}\frac{\partial\boldsymbol{G}}{\partial\kappa_i}, \tag{31}$$

where

$$\boldsymbol{J}=\begin{bmatrix}\boldsymbol{C}&\boldsymbol{0}&\boldsymbol{0}&\boldsymbol{0}&\boldsymbol{0}&\boldsymbol{S}\\ \boldsymbol{D}&\boldsymbol{A}-\widetilde{\sigma}_{\mathrm{m}}\boldsymbol{I}&\widetilde{\omega}_{\mathrm{m}}\boldsymbol{I}&-\widetilde{\boldsymbol{U}}_{\mathrm{Re}}&\widetilde{\boldsymbol{U}}_{\mathrm{Im}}&\boldsymbol{R}\\ \boldsymbol{D}'&-\widetilde{\omega}_{\mathrm{m}}\boldsymbol{I}&\boldsymbol{A}-\widetilde{\sigma}_{\mathrm{m}}\boldsymbol{I}&-\widetilde{\boldsymbol{U}}_{\mathrm{Im}}&-\widetilde{\boldsymbol{U}}_{\mathrm{Re}}&\boldsymbol{R}'\\ \boldsymbol{0}&\boldsymbol{U}^{\mathrm{T}}_{\mathrm{Re}}&\boldsymbol{U}^{\mathrm{T}}_{\mathrm{Im}}&0&0&0\\ \boldsymbol{0}&-\boldsymbol{U}^{\mathrm{T}}_{\mathrm{Im}}&\boldsymbol{U}^{\mathrm{T}}_{\mathrm{Re}}&0&0&0\\ \boldsymbol{0}&\boldsymbol{0}&\boldsymbol{0}&Y&Z&0\end{bmatrix}, \tag{32}$$

where $\boldsymbol{J}$ denotes the Jacobian matrix of $\boldsymbol{G}(\boldsymbol{y}_3)$, $\boldsymbol{C}$ and $\boldsymbol{S}$ represent the partial derivative matrixes of $\boldsymbol{F}_2$ in (13) with respect to $\widetilde{\boldsymbol{y}}_2$ and $\widetilde{\mu}$, respectively, Y and Z indicate the derivatives of (9f) with respect to $\widetilde{\sigma}_{\mathrm{m}}$ and $\widetilde{\omega}_{\mathrm{m}}$, respectively, $\boldsymbol{R}$ and $\boldsymbol{R}'$ denote the derivatives of (9b) and (9c) with respect to $\widetilde{\mu}$, respectively, which can be expressed as

$$\boldsymbol{R}=\frac{\partial\boldsymbol{A}}{\partial\widetilde{\mu}}\widetilde{\boldsymbol{U}}_{\mathrm{Re}},\boldsymbol{R}'=\frac{\partial\boldsymbol{A}}{\partial\widetilde{\mu}}\widetilde{\boldsymbol{U}}_{\mathrm{Im}}, \tag{33}$$

$\boldsymbol{D}$ and $\boldsymbol{D}'$ represent the derivatives of (9b) and (9c) with respect to $\widetilde{\boldsymbol{y}}_2$, respectively. For illustration, suppose that $\widetilde{y}^k_2$, $\widetilde{U}^j_{\mathrm{Re}}$, and $\widetilde{U}^j_{\mathrm{Im}}$ represent the kth, jth, and jth element of $\widetilde{\boldsymbol{y}}_2$,$\widetilde{\boldsymbol{U}}_{\mathrm{Re}}$, and $\widetilde{\boldsymbol{U}}_{\mathrm{Im}}$, respectively. D_{ik} and D'_{ik} indicate the elements at the ith row, kth column in matrixes $\boldsymbol{D}$ and $\boldsymbol{D}'$, respectively, and can be obtained by

$$D_{ik}=\sum_{j=1}^{N_{\mathrm{S}}}\left(\frac{\partial A_{ij}}{\partial\widetilde{y}^k_2}\widetilde{U}^j_{\mathrm{Re}}\right),D'_{ik}=\sum_{j=1}^{N_{\mathrm{S}}}\left(\frac{\partial A_{ij}}{\partial\widetilde{y}^k_2}\widetilde{U}^j_{\mathrm{Im}}\right). \tag{34}$$

The derivatives of the state matrix $\boldsymbol{A}$ with respect to arbitrary system parameters can be found in [36,37]. From (29)–(34), the computational requirement of the SSSM sensitivities are mainly concentrated in the formation and inverse of $\boldsymbol{J}$. In fact, only $\partial\widetilde{\mu}/\partial\kappa_i$ in $\partial\boldsymbol{y}_3/\partial\kappa_i$ is needed during the SSSMC-OPF solving process, the last row of the matrix $\boldsymbol{J}^{-1}$ formed when solving the SSSM with the Newton method can be used directly for calculating the SSSM sensitivities. The use of the Newton method to solve the SSSM facilitates the direct calculation of $\partial\gamma/\partial\kappa_i$.

It is worth pointing out that the derivative of SSSM (or $\boldsymbol{y}_3$) with respect to arbitrary operating parameters (e.g., nodal injection, PV-voltage) can be derived by the approach in (29)–(34).

5.5. Flowchart of the complete approach

For the sake of simplicity, a computational flowchart of the proposed approach for the SSSMC-OPF is given in Fig. 2. It consists of three core steps: calculating the augmented Lagrangian function, updating $\boldsymbol{H}^{(l)}$ with the BFGS technique, and one-dimensional search. The computational burden is mainly concentrated in the third step, as the SSSM index is repeatedly computed. In this paper, the 3-stage strategy is utilized to compute the SSSM, where the Newton method is used in the second stage. A detailed description of the 3-stage strategy can be found in [23].

6. Case studies

In this section, the proposed approach is applied to an 8-machine 24-bus system and a modified practical 68-machine 2395-bus system to illustrate the effectiveness. For all systems, the generators are described by the sixth-order model [38]. Except for the equivalent generator, all the generators are equipped with excitation system, turbine governor, and PSS. The loads are modeled as constant impedance. Assuming that all loads are increased by the same percentage from the initial operating point [20,22–24,28], the amount of load increase is distributed to all generators at the marginal cost of generation.

The adopted computing platform is a personal workstation with 2.4-GHz Intel Xeon Silver 4214R CPU and 32 GB RAM. The runtime environment is Visual Fortran 11.0. The damping ratio threshold ζ_{T} is set to be 3 %. The convergence tolerance for both the proposed approach and the 3-stage strategy is set to be 10^{-6}.

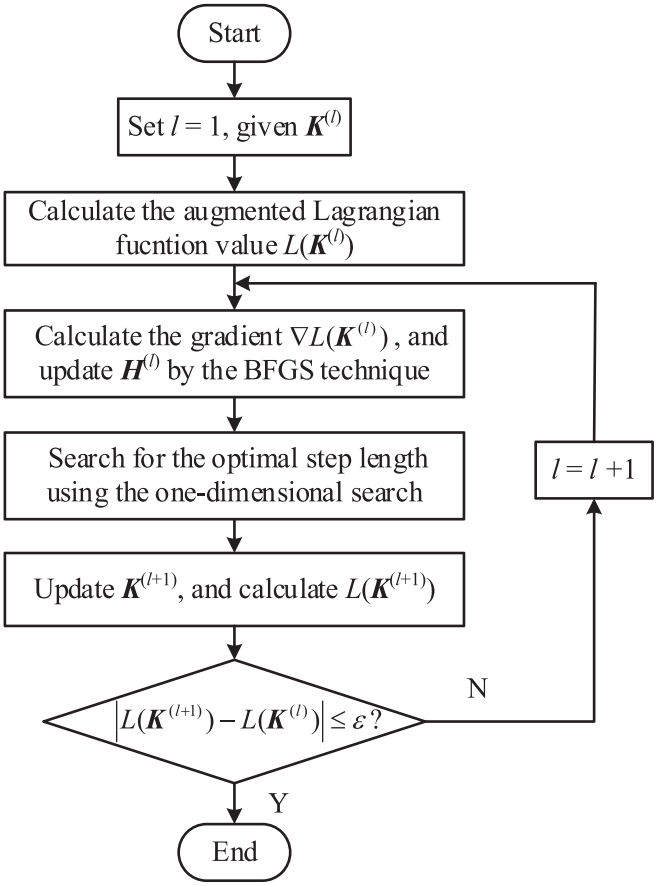

Fig. 2. Flowchart of the proposed approach for SSSMC-OPF.

6.1. 8-Machine 24-bus system

The 8-machine 24-bus system of Fig. 3 is often used for small-signal stability analysis [35–37,39–41]. Details of network parameters, nodal powers, and control system parameters can be found in [41]. The generator cost coefficients are listed in Table 2. Since the slack generator G8 can be regarded as an equivalent generator, the lower and upper limits of active power for G8 are 100 MW and 1000 MW, respectively, the lower and upper limits of active power for the remaining generators are 100 MW and 600 MW, respectively; the lower limit of reactive power of all generators is −100 MVar, the upper limits of reactive power for the slack generator and the remaining generators are 484.32 MVar and 371.85 MVar, respectively. The acceptable voltage magnitudes of all buses can vary between 1.05 p.u. and 0.95 p.u.

1) Comparison of the modified SSSM model and SSSM model

In the 8-machine system, there are 114 state variables and 189 non-state variables. The minimum damping ratio of the initial operating state is 3.30 %, and the corresponding mode is $-0.1269 \pm j3.8397$. Whether the SSSM model or the modified SSSM mode is used, the computed SSSM index γ by the 3-stage strategy is 58.11 %. However, solving the SSSM model takes 6.27 s, while solving the modified SSSM model takes only 3.08 s. This is because ineffective controller equations under steady-state are not included in the modified SSSM model.

The number of equations in the SSSM model is 534. Using the approach described in Section 3.3, the number of equations in the modified SSSM model is 333. Compared with the SSSM model, the number of equations in the modified SSSM model is reduced by 201.

2) Verification of SSSM sensitivities

In order to verify the derived analytical representation of SSSM sensitivities, the SSSM sensitivities computed from the analytical approach and the numerical approach are listed in Table 3. In the table, the superscript "N" has been dropped for convenience, $\dot{\gamma}_a$ is obtained using the analytical representation of (29)–(34), while $\dot{\gamma}_n$ is computed from the numerical calculation of either $\Delta\gamma/\Delta P_{Gi}^N$ or $\Delta\gamma/\Delta V_{Gi}^N$. It can be observed that $\dot{\gamma}_n$ and $\dot{\gamma}_a$ have the same sign and are on the same order of magnitude. This indicates that the analytical representation of SSSM sensitivities is accurate and can be utilized to guide the optimization direction of the SSSMC-OPF.

3) Effectiveness of the proposed approach

To analyze the effectiveness of the proposed approach, OPF results with and without SSSM constraints are listed in Table 4, where L denotes the augmented Lagrangian function value, ζ_{min} and λ_{min} represent the minimum damping ratio and the corresponding eigenvalue, respectively. From rows 2 and 3 of Table 4, the augmented Lagrangian function value is reduced from 34148.43 to 31060.18 and the minimum damping ratio decreases from 3.30 % to 2.78 %. Since the minimum damping ratio in the standard OPF results is less than 3 %, the SSSM index is 0. The results indicate that the standard OPF may result in a decrease in the SSSM index or even fail to meet requirements.

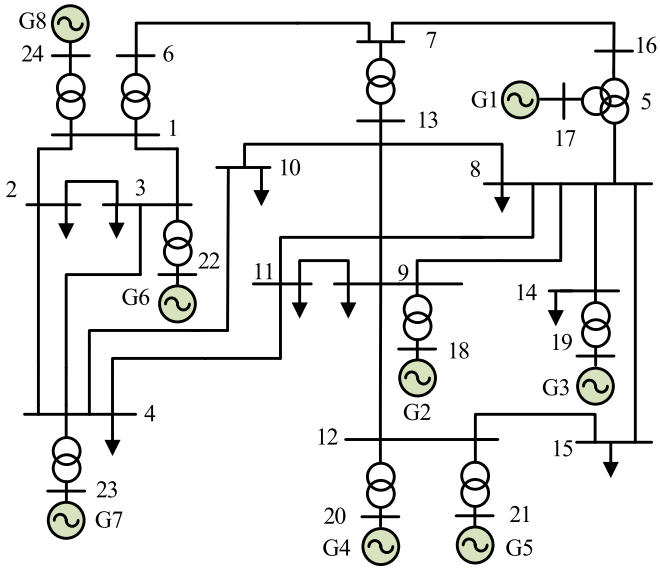

Fig. 3. Network diagram of the 8-machine 24-bus system.

Table 2
Generation Cost Coefficients for 8-Machine 24-Bus System.

Generator No.	a ($/MW^2)	b ($/MW)	c ($)
1	5.04×10^{-3}	2.00	1200.64
2	2.00×10^{-2}	5.00	1857.20
3	1.47×10^{-2}	4.20	1625.92
4	1.18×10^{-2}	3.64	1395.19
5	1.62×10^{-2}	2.57	1651.55
6	7.79×10^{-3}	3.11	1611.39
7	1.67×10^{-2}	2.24	1810.83
8	1.66×10^{-2}	3.46	1486.81

Table 3
SSSM Sensitivities to Active Injections and Voltage Magnitudes at Generator Buses for 8-Machine 24-Bus System.

Variable	$\dot{\gamma}_a$	$\dot{\gamma}_n$	Variable	$\dot{\gamma}_a$	$\dot{\gamma}_n$
P_{G1}	−0.167724	−0.167756	V_{G1}	2.228889	1.790832
P_{G2}	−0.044616	−0.044647	V_{G2}	−0.211474	−0.273715
P_{G3}	−0.066279	−0.066298	V_{G3}	−0.035514	−0.072762
P_{G4}	−0.140628	−0.140646	V_{G4}	0.705065	0.624830
P_{G5}	−0.118153	−0.118167	V_{G5}	0.506030	0.430408
P_{G6}	−0.021048	−0.021052	V_{G6}	−0.109228	−0.109346
P_{G7}	−0.030425	−0.030432	V_{G7}	0.056975	0.041853

Table 4
OPF Results with and Without SSSM Constraints for 8-Machine 24-Bus System.

	L	SSSM	ζ_{min}	λ_{min}
Initial state	34148.43	58.11 %	3.30 %	$-0.1269 \pm j3.8397$
Standard OPF	31060.18	0	2.78 %	$-0.1091 \pm j3.9173$
$\gamma \geq 35$ %	31122.34	35.31 %	3.39 %	$-0.1318 \pm j3.8872$
$\gamma \geq 40$ %	31855.89	40.05 %	3.36 %	$-0.1304 \pm j3.8764$
$\gamma \geq 45$ %	32698.98	45.00 %	3.36 %	$-0.1316 \pm j3.9148$

It can be observed from rows 3 and 4 of Table 4 that the critical mode of OPF and OPF with $\gamma \geq 35$ % are the same mode, the difference in the augmented Lagrangian function value is only 62.16. However, the minimum damping ratio at the optimal operating point obtained from OPF with $\gamma \geq 35$ % is satisfied, and the SSSM index is 35.31 %. This is because the SSSM constraint plays an important role in the optimization. For OPF with $\gamma \geq 35$ %, curves of the augmented Lagrangian function value L and SSSM with iterations are given in Fig. 4, variations of the minimum damping ratio ζ_{min} and the corresponding mode λ_{min} with iterations are given in Table 5. From Fig. 4 and Table 5, both the minimum damping ratio and the SSSM index are satisfied in the optimization process. It can also be observed that neither the minimum damping ratio nor the SSSM index varies monotonically during the optimization process. This phenomenon is related to the selection of initial values (e.g., control variables, penalty factors).

From rows 4 to 6 of Table 4, it can be observed that the optimization results all satisfy the SSSM requirements, and minimum operating cost and maximum SSSM index are in conflict. The larger the SSSM threshold, the higher the generation cost. Detailed results of initial state, standard OPF, and OPF with $\gamma \geq 45$ % are provided by Table 6. From the comparison of the initial state and the standard OPF, it can be observed that the changes in the active power output of G1 and G2 are relatively large, where the active power output of G1 increases by 2 p.u. to reach the upper limit, and the active power output of G2 decreases by 2.9206

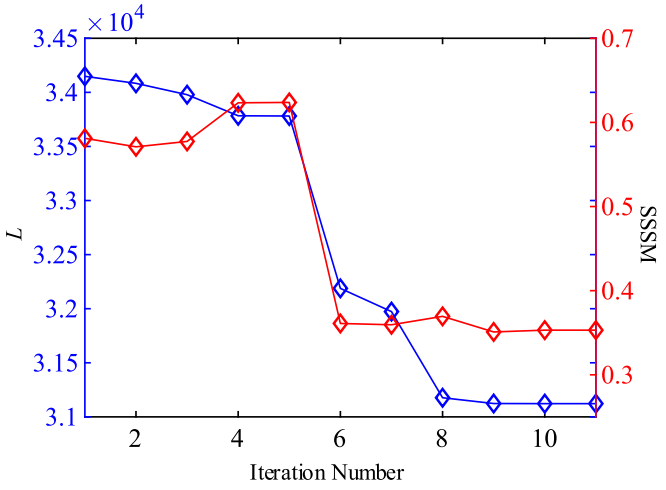

Fig. 4. Curves of the augmented Lagrangian function value L and SSSM with iterations under $\gamma \geq 35$ % for 8-machine 24-bus system.

Table 5
Variations of $\zeta_{\min}$ and $\lambda_{\min}$ under $\gamma \geq 35$ % for 8-Machine 24-Bus System.

Iter.	$\lambda_{\min}$	$\zeta_{\min}$	Iter.	$\lambda_{\min}$	$\zeta_{\min}$
1	$-0.1269 \pm j3.8397$	3.30 %	7	$-0.1339 \pm j3.9238$	3.41 %
2	$-0.1287 \pm j3.8524$	3.34 %	8	$-0.1321 \pm j3.8525$	3.42 %
3	$-0.1293 \pm j3.8514$	3.35 %	9	$-0.1331 \pm j3.8835$	3.42 %
4	$-0.1260 \pm j3.8788$	3.24 %	10	$-0.1318 \pm j3.8872$	3.39 %
5	$-0.1259 \pm j3.8797$	3.24 %	11	$-0.1318 \pm j3.8872$	3.39 %
6	$-0.1312 \pm j3.9240$	3.34 %			

p.u. This is because G1 has the cheapest marginal cost of generation and G2 has the highest marginal cost of generation, as shown in Table 2. From the comparison of the standard OPF and OPF with $\gamma \geq 45$ % in Tables 4 and 6, it can be observed that in order to meet the SSSM requirement, the active power output and voltage magnitude of the generators have changed, resulting in the value of the augmented Lagrangian function increased by 5.28 %.

From the active power output at the optimal operating point and the corresponding critical operating point, i.e., P_{Gi}^{N} and P_{Gi}^{C} in OPF with $\gamma \geq 45$ %, it can be observed that the critical operating point is obtained when the nodal voltages of all generators are kept constant and the total generation increases from 26.8259 p.u. to 39.1142 p.u.

6.2. A modified practical system

The modified practical system shown in Fig. 5 [38] consists of 68 synchronous machines, 2395 buses, 5488 transmission lines, 1496 transformers, and 458 constant impedance loads, of which 57 generators can be rescheduled. The total active and reactive load power are 35244 MW and 11199.41 MVar, respectively. Details of network parameters, nodal powers, and control system parameters can be found in commercial software PSASP (Power System Analysis Software Package) [38].

In this case, the total number of state and non-state variables is 1220 and 6461, respectively. The number of equations in the SSSM model is 10124, while the number of equations in the modified SSSM model is 7707. Compared with the SSSM model, the number of equations in the modified SSSM model is reduced by 2417.

OPF results with and without SSSM constraints are shown in Table 7. Taking OPF with $\gamma \geq 10$ % as an example, curves of the augmented Lagrangian function value L and SSSM with iterations are given in Fig. 6. It can be observed from rows 2 and 3 of Table 7 that by solving standard OPF model, the augmented Lagrangian function value is decreased from 159110.21 to 114303.84. However, the minimum damping ratio of the operating point is reduced from 4.09 % to −0.62 %, resulting in a SSSM of 0. From Fig. 6 and rows 3 and 4 of Table 7, it can be seen that compared with standard OPF, SSSMC-OPF has relatively high operating cost, but effectively ensures the minimum damping ratio and SSSM index of the operating point. It can also be observed from rows 4 and 5 of Table 7 that the generation cost increases with more tightened SSSM constraint. Compared to the standard OPF, the augmented Lagrangian function value obtained from OPF with $\gamma \geq 14$ % is increased by 2.73 %, but the optimal operating point can withstand a load increase of 5078.66 MW and 1613.83 MVar along the given direction of power variation to reach the critical operating point.

7. Conclusion

An OPF technique with exact SSSM constraint is described in this paper. The SSSM is measured by the percentage change in the total active load for a given direction of power variation that would cause the damping ratio to reach its minimum limit. A modified SSSM model is then proposed to reduce the computational requirement for practical studies. Subsequently, an OPF model with the SSSM inequality constraint is established and solved by a joint solution approach, where the analytical representation of the SSSM sensitivities is derived and utilized to guide the optimization direction. The use of the modified SSSM model and the three-stage strategy facilitates the direct calculation of SSSM derivatives. Finally, case studies on the 8-machine 24-bus system and the modified practical 68-machine 2395-bus system show that the generation costs of the SSSMC-OPF are only 5.28 % and 2.73 % higher than those of the OPF, while the SSSMs are improved by 45 % and 14.41 %, respectively. Simulation results demonstrate that the proposed approach can be effectively used for adjusting the system operating point to minimize the generation cost while retaining sufficient small-signal stability margin.

It is worth pointing out that in the proposed SSSMC-OPF model, the direction of load and generation variation is specified. The worst-case direction of power variation is more reasonable when the direction of power variation cannot be accurately determined or when uncertainty is considered. For high renewable energy penetrated power systems, the SSSMC-OPF considering the worst-case direction of power increase will

Table 6
Detailed Results of Initial state, Standard OPF, and OPF with $\gamma \geq 45$ % for 8-Machine 24-Bus System.

Generator No.	Initial state			Standard OPF			OPF with $\gamma \geq 45$ %				
	P_{Gi}^{N} (p.u.)	Q_{Gi}^{N} (p.u.)	V_{Gi}^{N} (p.u.)	P_{Gi}^{N} (p.u.)	Q_{Gi}^{N} (p.u.)	V_{Gi}^{N} (p.u.)	P_{Gi}^{N} (p.u.)	Q_{Gi}^{N} (p.u.)	V_{Gi}^{N} (p.u.)	P_{Gi}^{C} (p.u.)	Q_{Gi}^{C} (p.u.)
1	4.0000	1.2990	1.0000	6.0000	1.6571	0.9883	4.5646	0.4969	0.9560	7.6237	3.8503
2	4.6000	1.1033	1.0000	1.6794	0.4768	1.0005	3.5849	0.8248	1.0019	4.2252	2.0824
3	2.3000	2.4330	1.0000	2.5047	1.8338	0.9510	2.4282	2.2801	0.9793	3.7744	4.5236
4	3.2500	0.7777	1.0000	3.1768	1.5297	1.0326	3.2827	1.2826	1.0477	4.9398	2.8372
5	3.0600	0.8781	1.0000	2.6139	0.1691	0.9788	2.9887	1.4985	1.0461	4.3353	3.3203
6	4.0000	3.5753	1.0000	5.3422	3.4606	0.9953	4.3555	3.1721	0.9689	7.1780	5.7085
7	3.1000	3.1202	1.0000	2.8163	2.8719	0.9884	3.0960	2.7864	0.9756	4.5757	5.5817
8	2.5748	0.5705	0.9700	2.6033	0.7621	0.9700	2.5253	0.9537	0.9700	2.4621	3.0115

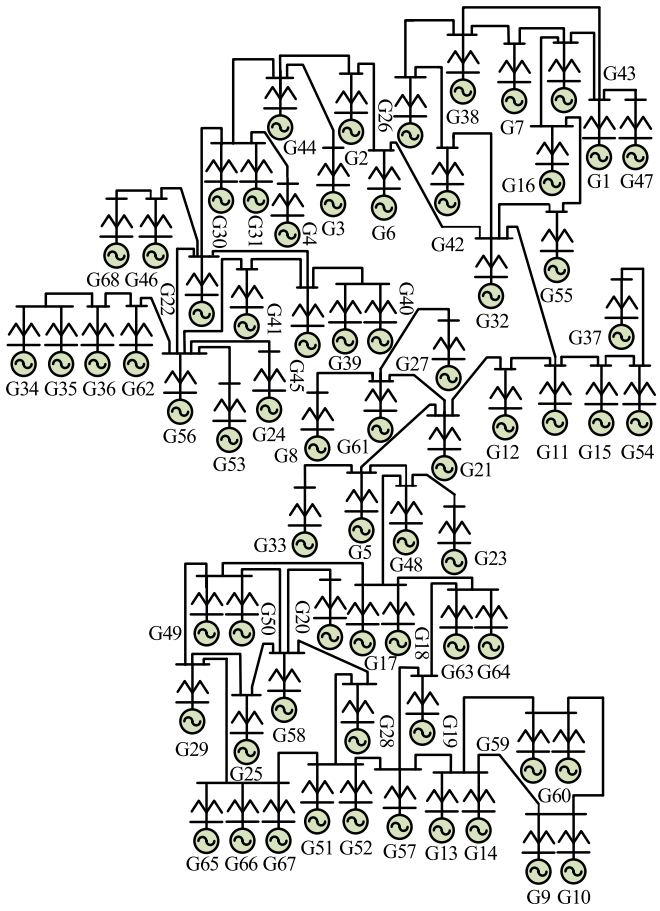

Fig. 5. Network diagram of the modified practical 68-machine 2395-bus system.

Table 7
OPF Results with and Without SSSM Constraints for 68-Machine 2395-Bus System.

	L	SSSM	$\zeta_{\min}$
Initial state	159110.21	10.51 %	4.09 %
Standard OPF	114303.84	0	−0.62 %
$\gamma \geq 10$ %	115577.68	10.42 %	4.14 %
$\gamma \geq 14$ %	117427.77	14.41 %	4.49 %

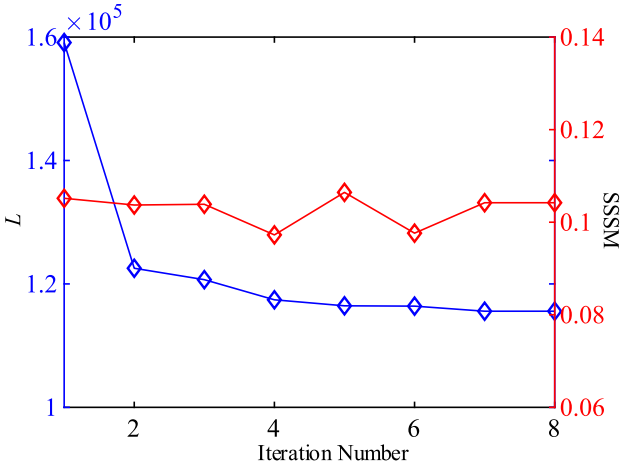

Fig. 6. Curves of the augmented Lagrangian function value L and SSSM with iterations under $\gamma \geq 10$ % for 68-machine 2395-bus system.

be investigated in the future.

CRediT authorship contribution statement

Zheng Huang: Writing – review & editing, Writing – original draft, Visualization, Software, Methodology, Formal analysis, Data curation. **Kewen Wang:** Writing – review & editing, Supervision, Project administration, Conceptualization. **Yi Wang:** Writing – review & editing, Funding acquisition. **Fushuan Wen:** Writing – review & editing. **Venkata Dinavahi:** Writing – review & editing. **Jun Liang:** Writing – review & editing, Supervision.

Declaration of competing interest

The authors declare that they have no known competing financial interests or personal relationships that could have appeared to influence the work reported in this paper.

Acknowledgements

This work was supported in part by the National Natural Science Foundation of China under Grant 62203395, in part by the Special Financial Grant from the China Postdoctoral Science Foundation under Grant 2023TQ0306, and in part by the Postdoctoral Research Project of Henan Province under Grant 202101011.

Data availability

The authors do not have permission to share data.

References

[1] Hao GT, Han XS, Luo SB, Ye PF, Wen H. Decentralized DC optimal power flow model based on improved Lagrangian and consensus algorithm. Int J Electr Power Energy Syst 2024;155:109555.
[2] Norouzi M, Aghaei J, Pirouzi S, Niknam T, Fotuhi-Firuzabad M. Flexibility pricing of integrated unit of electric spring and EVs parking in microgrids. Energy 2022; 239:122080.
[3] Liang HJ, Pirouzi S. Energy management system based on economic Flexi-reliable operation for the smart distribution network including integrated energy system of hydrogen storage and renewable sources. Energy 2024;293:130745.
[4] Qu ZY, Xu CF, Yang F, Ling F, Pirouzi S. Market clearing price-based energy management of grid-connected renewable energy hubs including flexible sources according to thermal, hydrogen, and compressed air storage systems. J Energy Storage 2023;69:107981.
[5] Zhang XW, Yu XP, Ye XP, Pirouzi S. Economic energy management of networked flexi-renewable energy hubs according to uncertainty modeling by the unscented transformation method. Energy 2023;278:128054.
[6] Kazemi M, Salehpour SY, Shahbaazy F, Behzadpoor S, Pirouzi S, Jafarpour S. Participation of energy storage-based flexible hubs in day-ahead reserve regulation and energy markets based on a coordinated energy management strategy. Int Trans Electr Energy Syst 2022;2022:1–17.
[7] Khalafian F, Iliaee N, Diakina E, Parsa P, Alhaider MM, Masali MH, et al. Capabilities of compressed air energy storage in the economic design of renewable off-grid system to supply electricity and heat costumers and smart charging-based electric vehicles. J Energy Storage 2024;78:109888.
[8] Wang J, Song Y, Hill DJ, Hou YH. Preventive–corrective stability constrained OPF in microgrids for accommodating DG plug-and-play. Int J Electr Power Energy Syst 2024;155:109646.
[9] Gan D, Thomas RJ, Zimmerman RD. Stability-constrained optimal power flow. IEEE Trans Power Syst 2000;15(2):535–40.
[10] Kim MK, Hur D. Decomposition–coordination strategy to improve power transfer capability of interconnected systems. Int J Electr Power Energy Syst 2011;33: 1638–47.
[11] Chung CY, Wang L, Howell F, Kundur P. Generation rescheduling methods to improve power transfer capability constrained by small-signal stability. IEEE Trans Power Syst 2004;19(1):524–30.
[12] Condren J, Gedra T. Expected-security-cost optimal power flow with small-signal stability constraints. IEEE Trans Power Syst 2006;21(4):1736–43.
[13] Inoue M, Sadamoto T, Arahata M, Chakrabortty A. Optimal power flow design for enhancing dynamic performance: potentials of reactive power. IEEE Trans Smart Grid 2020;12(1):599–611.
[14] Li P, Qi J, Wang J, Wei H, Bai X, Qiu F. An SQP method combined with gradient sampling for small-signal stability constrained OPF. IEEE Trans Power Syst 2017; 32(3):2372–81.

[15] Li Y, Geng G, Jiang Q, Li W, Shi X. A sequential approach for small signal stability enhancement with optimizing generation cost. IEEE Trans Power Syst 2019;34(6):4828–36.
[16] Pareek P, Nguyen HD. A convexification approach for small-signal stability constrained optimal power flow. IEEE Trans Control of Network Syst 2021;8(4):1930–41.
[17] Pullaguram D, Madani R, Altun T, Davoudi A. Small-signal stability-constrained optimal power flow for inverter dominant autonomous microgrids. IEEE Trans Indust Electron 2022;69(7):7318–28.
[18] Yang ZQ, Lin SJ, Yang YR, Chen SY, Liu M. Small-signal stability constrained optimal power flow of power system with DFIGs considering wind power uncertainty. Int J Electr Power Energy Syst 2023;154:109467.
[19] Liu J, Yang Z, Zhao J, Yu J, Tan B, Li W. Explicit data-driven small-signal stability constrained optimal power flow. IEEE Trans Power Syst 2022;37(5):3726–37.
[20] Azad SP, Iravani R, Tate JE. Dynamic stability enhancement of a DC-segmented AC power system via HVDC operating-point adjustment. IEEE Trans Power Delivery 2015;30(2):657–65.
[21] Makarov YV, Dong ZY, Hill DJ. A general method for small signal stability analysis. IEEE Trans Power Syst 1998;13(3):979–85.
[22] Wen X, Ajjarapu V. Application of a novel eigenvalue trajectory tracing method to identify both oscillatory stability margin and damping margin. IEEE Trans Power Syst 2006;21(2):817–24.
[23] Li C, Chiang HD, Du Z. Investigation of an effective strategy for computing small-signal security margins. IEEE Trans Power Syst 2018;33(5):5437–45.
[24] Rosehart WD, Canizares CA, Quintana VH. Multiobjective optimal power flows to evaluate voltage security costs in power networks. IEEE Trans Power Syst 2003;18(2):578–87.
[25] Gholizadeh A, Abbas R, Fadaeinedjad R. A scenario-based voltage stability constrained planning model for integration of large-scale wind farms. Int J Electr Power Energy Syst 2019;105:564–80.
[26] Hamon C, Perninge M, Söder L. A stochastic optimal power flow problem with stability constraints—Part I: approximating the stability boundary. IEEE Trans Power Syst 2013;28(2):1839–48.
[27] Perninge M, Hamon C. A stochastic optimal power flow problem with stability constraints—Part II: the optimization problem. IEEE Trans Power Syst 2013;28(2):1849–57.
[28] Ajjarapu V, Christy C. The continuation power flow a tool for steady state voltage stability analysis. IEEE Trans Power Syst 1992;7(1):416–23.
[29] Pirouzi S. Network-constrained unit commitment-based virtual power plant model in the day-ahead market according to energy management strategy. IET Gener Transm Distrib 2023;17:4958–74.
[30] Norouzi M, Aghaei J, Niknam T, Pirouzi S, Lehtonen M. Bi-level fuzzy stochastic-robust model for flexibility valorizing of renewable networked microgrids. Sustain Energy Grids Netw 2022;31:100684.
[31] Kundur P. Power system stability and control. New York: McGrawHill; 1994.
[32] Frank S, Steponavice I, Rebennack S. Optimal power flow: a bibliographic survey I. Energy Syst 2012;3:221–58.
[33] Frank S, Steponavice I, Rebennack S. Optimal power flow: a bibliographic survey II. Energy Syst 2012;3:259–89.
[34] Nocedal J, Wright SJ. Numerical optimization. 2nd ed. New York: Springer; 2006.
[35] Chung CY, Wang KW, Tse CT, Bian XY, David AK. Probabilistic eigenvalue sensitivity analysis and PSS design in multimachine systems. IEEE Trans Power Syst 2003;18(4):1439–45.
[36] Wang KW, Chung CY, Tse CT, Tsang KM. Multimachine eigenvalue sensitivities of power system parameters. IEEE Trans Power Syst 2000;15(2):741–77.
[37] Wang KW, Chung CY, Tse CT, Tsang KM. Improved probabilistic method for power system dynamic stability studies. IEE Proc Gener Transm Distrib 2000;147(1):37–43.
[38] Zhongxi W, Xiaoxin Z. Power system analysis software package (PSASP)-an integrated power system analysis tool. In: POWERCON'98. 1998 International Conference on Power System Technology. Proceedings (Cat. No. 98EX151), Vol. 1. IEEE; 1998. p. 7–11.
[39] Bian XY, Geng Y, Lo KL, Fu Y, Zhou QB. Coordination of PSSs and SVC damping controller to improve probabilistic small-signal stability of power system with wind farm integration. IEEE Trans Power Syst 2016;31(3):2371–82.
[40] He P, Wen FS, Ledwich G, Xue YS. An investigation on interarea mode oscillations of interconnected power systems with integrated wind farms. Int J Electr Power Energy Syst 2016;78:148–57.
[41] Wang K.W., Robust P.S.S., Design Based on Probabilistic Approach. Ph.D. dissertation, Polytechnic University. Hong Kong, China, 2000.